NJC

New Journal of Chemistry

A journal for new directions in chemistry

Accepted Manuscript

This article can be cited before page numbers have been issued, to do this please use: M. R. Rodríguez, L. M. Balsa, J. Del Pla, J. García-Tojal , R. Pis Diez, B. S. Parajón Costa, I. Leon and A. C. González-Baró, *New J. Chem.*, 2019, DOI: 10.1039/C9NJ02092F.

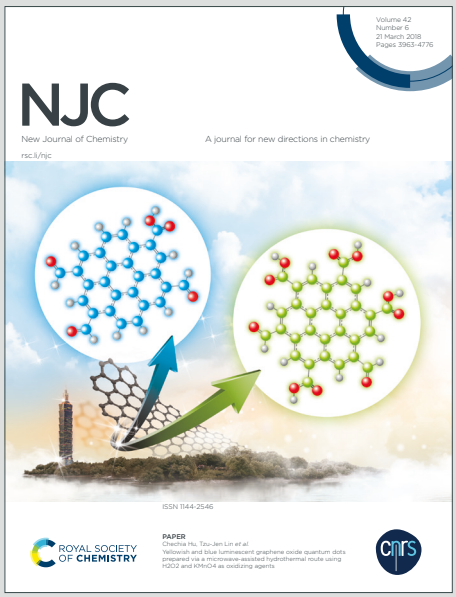

View Article Online
DOI: 10.1039/C9NJ02092F

Synthesis, characterization, DFT calculations and anticancer activity of an new Oxidovanadium(IV) complex with a ligand derived from *o*-vanillin and thiophene.

María R. Rodríguez [a], Lucía M. Balsa [a], Julián Del Plá [a], Javier García-Tojal [b], Reinaldo Pis-Diez [a], Beatriz S. Parajón-Costa [a] Ignacio E. León [a*] and Ana C. González-Baró [a *]

[a] CEQUINOR (CONICET-CCT La Plata, UNLP), Bvd. 120 N°1465, B1900AVV La Plata, Argentina.

[b] Departamento de Química, UBU, Pza. Misael Bañuelos s/n, E-09001 Burgos, España.

Abstract

From the interaction of the vanadyl ion with a ligand (HL), obtained by the condensation reaction of *o*-vanillin and 2-thiophenemethylamine, a oxodovanadium(IV) complex (VOL_2) is obtained. It is characterized by spectroscopic techniques, including solid state FTIR, Raman, EPR and diffuse reflectance and UV-vis and EPR in solutions. Its thermal behavior is analyzed by means of TGA and DTA. Theoretical studies based on DFT computational methods are of help in the interpretation and assignment of spectroscopic data. Cytotoxicity assays (48 h) against bone cancer cells (MG-63, IC_{50} = 50.4 ± 8.7), breast cancer cells (MCF-7, IC_{50} = 42.3 ± 4.7) and MDA-MB-231, IC_{50} = 29.0 ± 1.7) and a normal fibroblast (L929, IC_{50} = 71.0 ± 3.5), demonstrate the enhancement of effectiveness and selectivity of the complex compared with both the ligand and the free metal ion. Besides, the compound inhibits the cell migration, increases ROS level and conveys the cells to apoptosis. As a whole, these results show the main mechanisms of the deleterious effects of [VOL_2] in a triple negative breast cancer cell line (MDA-MB-231), demonstrating that this complex is a promising therapeutic agent for this kind of breast cancer.

1. Introduction

Among the transition metals with biological and therapeutic relevance, vanadium is recognized for the wide range of biological roles and therapeutic activities involving its various oxidation states and specially as V(IV) and V(V).[1,2] As such a versatile metal ion, that can act either as an anion or as a cation, vanadium promotes a extensive chemistry and biochemistry, depending on its oxidation state and the electronic and nature of the coordinating ligands.[3]

View Article Online
DOI: 10.1039/C9NJ02092F

In particular, its coordination chemistry has been extensively explored and some examples of the interesting properties of vanadium complexes can be found in the literature.[4-6] Among the variety of therapeutic activities, it appears that vanadium suppresses growth and spread of tumors by inhibiting cell proliferation, inducing apoptosis, and limiting invasion and the metastatic potential of neoplastic cells. The vanadium involvement in redox-active ROS-RNS associated apoptotic processes, interactions with mi RNA, autophagy and cell differentiation capacities, denotes the potential of this metal as a promising anticancer metallodrug.[7]

It is expected that the interaction of this bio-metal with active ligands leads to an improvement in the activity of the ligand or the metal themselves, as it has been extensively described. Ligands can moderate the adverse effects of metal ion, inhibit selected metalloenzymes or assist in metal ion distribution. Some of these effects imply modifying reactivity and lipophilicity, stabilizing specific oxidation states, and contributing to substitution inertness.[8]

Furthermore, vanadium has been important in the development of metallo-pharmaceuticals with diverse therapeutic activity in an attempt to lower the side effects. In this sense, the design and synthesis of suitable multidentate ligands provide a significant contribution to the therapeutic aspect of vanadium coordination chemistry.[9]

The interest in combining a metal with poly-functional ligands having diverse potentially coordinating donor atoms is based on the structural versatility, syntheses accessibility and wide application of the metal complexes in different fields including food and dye industries or analytical and agro-chemistry and also due to their catalytic, antioxidant, fungicidal, anti-inflammatory and antitumor activities [10-12]

These chelating ligands can be designed combining precursor reactants that provide active scaffolds to the product. In the present work, the selected ligand HL (oVATPNH2 , see Figure 1) is an example of Schiff base derived from primary amines involving a heterocycle and has been obtained and fully characterized in our laboratory.[13] It is the condensation product of o-vanillin (2-hydroxy-3-methoxybenzaldehyde, hereafter oHVa) and 2-thiophenemethylamine (TPNH2).

The involvement of the different heterocyclic, including thiophene, in the structure of organic molecules suitable for metal coordination, has been a successful strategy in the development of new drugs. Many of them have shown a wide range of pharmacological effects, such as antimicrobial, anthelmintic, anti-inflammatory, analgesic, antipyretic, diuretic, hypoglycemic, anticonvulsant, anti-HIV, cytotoxic and antitumor activities.[14,15] In particular, participation of thiophene in Schiff bases are of special interest because of the improvement of therapeutic agents capacity.[16] Hence, compounds derived from this ring are good candidates for ligands in potentially active metal complexes, regardless the coordination capacity of the heteroatom. Furthermore, oHVa has demonstrated an antioxidant capacity even higher that of its positional isomer, the well-known natural flavoring agent vanillin.[17]

View Article Online
DOI: 10.1039/C9NJ02092F

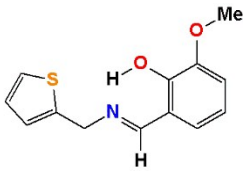

Figure 1:oVATPNH2 ligand (2-methoxy-6-{(*E*)-[(thiophen-2-ylmethyl)imino]methyl}phenol).

Ligands belonging to the Schiff bases family can coordinate metal centers through the N atom in the azomethine >C=N- moiety, a functional group that is strongly believed to play an important role in a broad variety of biological activities, including antibacterial, antitumor, antifungal or antimalarial. Although the imine nitrogen atom itself is capable of acting as a coordinating donor atom, stability is enhanced when the metal ion is coordinated with other electron donating groups of the molecule giving rise to a five or six-membered chelate ring (coordination ring). This condition is generally reached when other electron donating groups, either as ring heteroatoms or as substituents on molecular scaffold, are present in the vicinity of the azomethine linkage.[18]

Within the multiplicity of therapeutic properties of metal complexes, anticancer activity is one of the most significant.[19] In particular, breast cancer is one of the more frequent causes of premature mortality in female population. One of the most aggressive types is the one known as triple-negative breast cancer. Up to the moment, chemotherapy seems to be the only possible treatment, involving side effects. Then, great efforts are devoted to improving therapeutic agents to optimize the treatment. [20]

Recently, we have reported the Zn(II) and Cu(II) complexes with oVATPNH2 in the same coordination fashion that in the present oxidovanadium(IV) compound and also with formula ML_2.[21] The structural data, obtained by RDX of monocrystals, was of help in the analysis of the vanadium complex, despite the difference in the environments geometry. The copper complex proved to be active against two breast cancer cells, with IC_{50} values lower than those of cisplatin. This result encouraged us to continue in the search of new agents against breast adenocarcinoma, involving metals less toxic than platinum.

~~The interaction of oVATPNH2 with oxidovanadium(IV) acetylacetonate leads to the formation of the stable complex [VO(oVATPNH2)$_2$] (see Scheme 2)~~.

View Article Online
DOI: 10.1039/C9NJ02092F

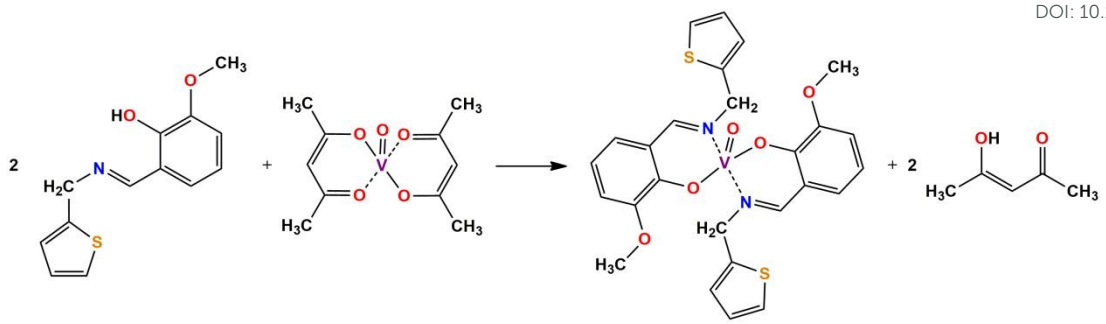

Scheme 1: Formation reaction of the complex [VO(oVATPNH2)$_2$].

The complex is obtained according the reaction depicted in Scheme 1. It is fully characterized by means of spectroscopic (FTIR, Raman, UV-Vis, diffuse reflectance and EPR) techniques and its thermal behavior has been explored by TGA and DTA. DFT calculations were performed to complement experimental results and to assist in their interpretation. The cytotoxic activity of the complex is essayed against three tumoral cell lines (MG-63, MCF7, MDA-MB-231) and one normal cell line (L929) and compare with the free ligand and metal ions. Besides, the cell migration, the ROS production and apoptosis induction is studied in an attempt to get information about the mechanisms of actions involved in the antitumor action of the complex. The physicochemical and structural analysis of the present compound can help in the understanding of its behavior in chemical or biological reactions, with relevance in the development of new therapeutic agents.

2. Results and discussion

2.1. DFT calculations and conformational analysis

Taking into account the similarities with previously studied Cu(II) and Zn(II) complexes with the same ligand [21] and the characterization results a square pyramidal environment was proposed for [VO(oVATPNH2)$_2$]. Despite the low quality of the crystals obtained prevented an acceptable X-ray structure determination and refinement, preliminary results agree with the proposed geometry. Thus, a square pyramidal environment with both ligands coordinating the vanadium center through the N and O donor atoms and the O atom of the oxovanadium moiety located at the apical position was used as the starting point in the conformational analysis.

The optimized geometry is depicted in Figure 2. The vanadium atom is coordinated by the two bidentate ligands in *trans* position building a nearly planar square O_2N_2 environment. The V atom lies approximately 0.6 Å over the plane and the O atom, located in the apical position, completes a distorted square-pyramidal coordination sphere.

View Article Online
DOI: 10.1039/C9NJ02092F

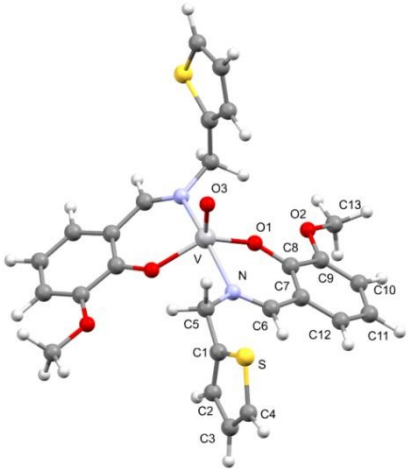

Figure 2. Optimized geometry of [VO(oVATPNH2)$_2$] showing the labeling of the non-H atoms for one of the ligands.

As can be seen in Figure 2, the S atoms do not participate in the coordination to the metal and the thiophene rings are orientated in *trans* position regarding the N_2O_2 pseudo-plane. In order to evaluate the possibility of π-interaction between the rings that can contribute to the structure stabilization, subsequent calculations were performed. A new geometry optimization, starting from a structure in which the thiophene rings are in a *cis* conformation allowing the mentioned interaction, leads to the structure depicted in Figure 3. Even though the energy calculated for the optimized *cis*-geometry (Figure 3, right) is only slightly higher than that calculated for the optimized *trans*-geometry (Figure 3, left) the relative orientation of the thiophene rings and the long distance between them are not compatible with the π-interactions.

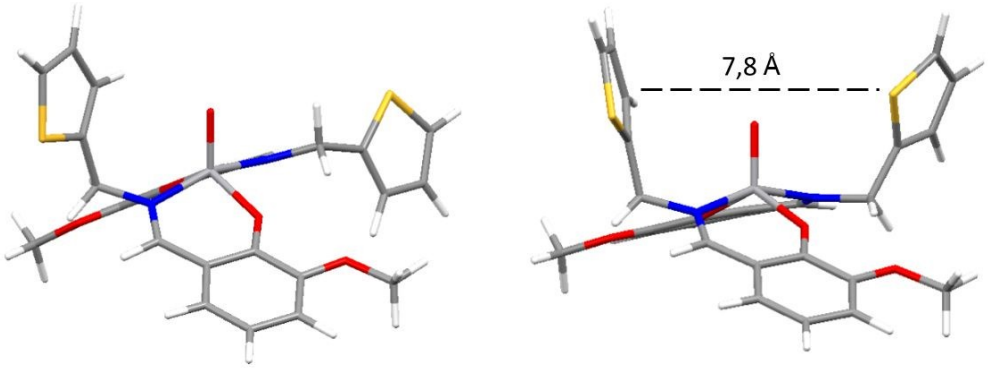

Figure 3. Optimized geometries of [VO(oVATPNH2)$_2$] taking different geometry as starting points. Left: thiophene rings in *trans* conformation. Right: thiophene rings in *cis* conformation. The distance between the thiophene rings is shown for the latter.

Considering these results and comparing them with those obtained for the Cu(II) and Zn(II) complexes crystal structures [21], we selected the *trans*-geometry to continue the study.

A list of the more relevant optimized geometrical parameters for the complex is available as ESI (Table S1). Calculations predict that the two ligands surrounding the metal ion are non-

View Article Online
DOI: 10.1039/C9NJ02092F

equivalent, thus giving two values for each geometrical parameter. For bond distances and bond angles, the difference among the two values for each ligand is small, and thus average values are listed in the table. Nevertheless, as significant differences are observed in calculated dihedral angles of the two ligands, both values are included.

Table 1 shows selected parameters involving the metal center. From previous results in other complexes using the same computational methodology bond distances and angles around metal ions are well described. Nevertheless, calculated N-M and O-M bond distances were slightly overestimated when compared with the crystallographic data.[21] Thus, it is expected that experimental N-V and V-O1 bond distances will be shorter than the values reported in Table 1.

Table 1. Selected geometrical calculated parameters involving the metal center for [VO(oVATPNH2)$_2$]

Bond distance (Å)		**Dihedral angle (º)**	
N-V	2.140	C5-N-V-O1	-179.2
V-O1	1.912	C5'-N'-V-O1'	-170.3
V-O3	1.603	C5-N-V-O1'	-56.9
		C5'-N'-V-O1	-47.5
Bond		C1-C5-N-V	173.7
C5-N-V	114.6	C8-O1-V-N	-2.3
C6-N-V	125.1	C8'-O1'-V-N'	-5.6
O1-V-N	86.6	C8-O1-V-N'	-171.0
O1-V-N'	85.8	C8'-O1'-V-N	-169.5
N-V-N'	163.6	C6-N-V-O1	6.4
O1-V-O1'	122.1	C6'-N'-V-O1'	1.7
O3-V-O1	119.8	C6-N-V-O1'	128.7
O3-V-N	98.0	C6'-N'-V-O1	124.6
C8-O1-V	135.2	C5-N-V-O3	58.2

2.2. Vibrational Spectroscopy

FTIR and Raman spectra of the complex were analysed in comparison with the spectra of the ligand that we have previously reported[18] and are shown in Figure 4. Assignments were done based on reported data,[22,23] results on related species[2,6,21,24] and with the help of DFT calculations. They are included in Table S2 (ESI) together with the complete spectroscopic results. Selected band positions, calculated frequencies and assignments are listed in Table 2.

As can be seen in the tables, calculations predicted a strong coupling of different modes at some frequencies.

View Article Online
DOI: 10.1039/C9NJ02092F

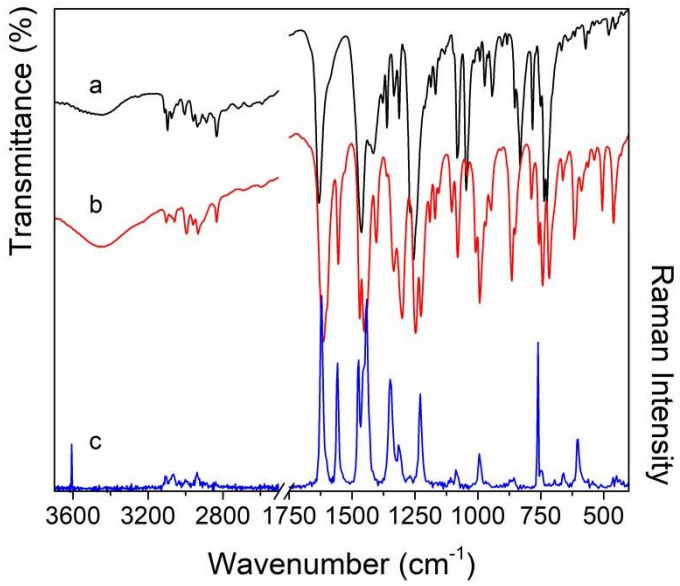

Figure 4. IR spectra of the ligand (a) and the complex (b). Raman spectrum of the complex (c).

Table 2. Vibrational spectra of the complex and the ligand. Selected experimental bands, calculated frequencies and assignemnts. Wavenummber in cm^{-1}.

oVATPNH2 (a)				VO(oVATPNH2)$_2$			
IR.	**Raman**	**Calc**	**Assignment**	**IR**	**Raman**	**Calc.**	**Assignment**
3003 vw	3005 w	3153	ν O-H				
1631 vs	1635 vs	1685	ν C=N	1613 vs	1621 vs	1677/1671	ν C=N
1583 sh	1587 m	1660/ 1618	ν ring (oVA) + δ O-H	1601 sh 1555 m	1558 s	1639/1636	ν ring (oVA)
1313 m		1315	ν C-O (ArOH)+ δ C-H(oVA)	1301 s,b	1312 m	1370/1349	ν C-O (Ar-O) + δ C-H (Ar-CH) + ρ_w CH_2
						1335	ν C-O(Ar-O) + ρ_w CH_2
832 ms,b	838 w	851	γ O-H				
						587	ν_{as} O-V-O + γring (Tph) + γ ring (oVA)
						581	ν_s O-V-O + δ Ar-OCH_3 + γ ring (Tph)
				461 w,b	467 sh	460/443	ν_{as} N-V-N
					444 w	464/455	ν_s N-V-N

(a) Data extracted from ref [13]. vs: very strong, s: strong, m: medium, w: weak, vw: very weak, b: broad, sh: shoulder: Tph: thiophene ring.

As expected, after the deprotonation of the phenolic group, the bands related to the O-H vibrations of the free ligand are absent in the spectra of the complexes. The strong C=N stretching band at 1631 cm^{-1} (IR) and 1635 cm^{-1} (Ra) in the ligand is shifted to lower frequencies (1613 and 1621 cm^{-1}, respectively) in the complex as a consequence of coordination to the metal through the N atom. Moreover, weak bands assigned to the symmetric and antisymmetric N-V-N stretchings are observed in the lower frequency region of the complex's spectra. The O-

View Article Online
DOI: 10.1039/C9NJ02092F

V-O stretching bands are predicted at higher wavenumbers as the calculated V-O distance is shorter than the V-N one, but they cannot be observed probably because they are overlapped with rings deformation modes. Additionally, the characteristic V=O band is observed at 993 cm^{-1} (IR) and 992 cm^{-1} (Ra).

The –N=C-C-C-O- moiety of each ligand bonded to the metal ion gives rise to a six-membered ring (coordination ring). In the complex, vibrations of these rings are predicted by calculations at lower frequencies that the respective modes of the ligand rings and coupled with them, giving rise to a shoulder in the IR and a red shift in the Raman spectrum, around 600 cm^{-1}. A similar behaviour has been observed in the previously studied related complexes. [21]

Modes related to the ligand rings vibrations and those assigned to the $–CH_2$ and $O-CH_3$ groups show minor changes in frequency and/or intensity upon coordination. For each mode of the ligand in the complex two close, or even coincident, values are calculated. This is explained by the prediction of two no strictly equivalent ligands in the environment of the metal centre.

2.3. EPR Spectroscopy.

The X-band EPR measurements on a polycrystalline solid of the complex (ESI, Figure S1) show slight variations of the spectra on decreasing temperature, which could be considered partially due to the broadening of the components of the hyperfine coupling with temperature. No wholly successful simulations are obtained for the spectrum at 120 K (see fitting parameters in Figure 5).

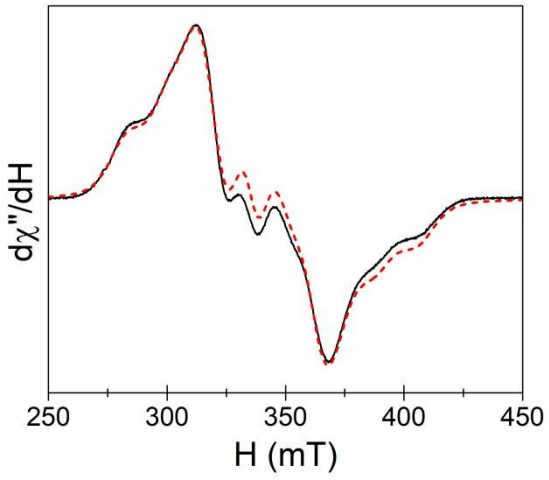

Figure 5. EPR experimental spectrum (solid line) and fit (dashed line) of $[VO(OVATPNH_2)_2]$ at room-temperature. Experimental details: modulation frequency = 100 kHz, modulation amplitude = 0.1 mT, time constant = 40.96 ms, conversion time = 327.68 ms, gain = 6,3 10^4, power = 2.0 mW, microwave frequency = 9.4223 GHz. Fitting parameters: (a) (Lorentzian/Gaussian) (1/1)-type signal, g_1 = 1.955; A_1 = 17.5 mT (159.7 x 10^{-4} cm^{-1}) (linewidth

View Article Online
DOI: 10.1039/C9NJ02092F

H_1 = 14.0 mT), g_2 = 1.984; A_2 = 6.1 mT (56.6 x 10^{-4} cm^{-1}) (linewidth H_2 = 11.0 mT), g_3 = 1.986; A_3 = 6.1 mT (56.5 x 10^{-4} cm^{-1}) (linewidth H_3 = 11.0 mT).

In order to complement the results for the solid sample, measurements in solution are carried out. Thus, a yellow solution of the complex in a (1:1) (ethanol:DMF) mixture of approximately 5 x 10^{-4} M is prepared, whose spectrum at 120 K and fitting are depicted in Figure 6. The spectrum evidences the presence of a unique V(IV) species. The average g and A values, 1.97 and 9.8 mT, respectively, agree well with those calculated from the measurements in solution at room temperature (1.974 and 9.9 mT, Figure S2 in ESI, Equations 1 and 2). On the other hand, the values of the parameters in frozen solution are similar to those in the solid state and suggest that the molecular structure is essentially retained in solution. In addition, these values evidence a rhombic symmetry in good agreement with the results of the computational studies, which provide three different metal-ligand average bond lengths around the V(IV) ions.

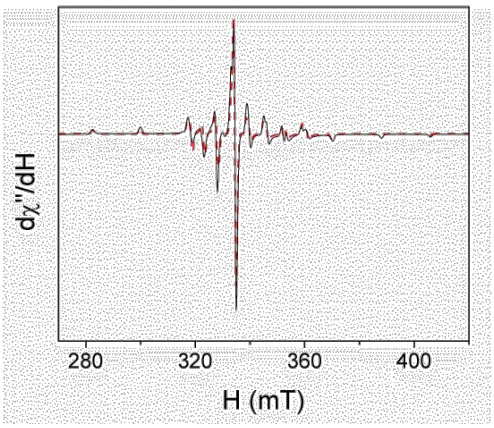

Figure 6. EPR spectrum of [$VO(OVATPNH_2)_2$] in solution in (1:1) (ethanol:DMF) at 120 K (solid line) together with the best fit (dashed line). Experimental details: modulation frequency = 100 kHz, modulation amplitude = 0.1 mT, time constant = 40.96 ms, conversion time = 327.68 ms, gain = 6.3 10^4, power = 20.0 mW, microwave frequency = 9.4185 GHz. Fitting parameters: Gaussian-type signal, second-order effects, g_1 = 1.955; A_1 = 17.6 mT (160.6 x 10^{-4} cm^{-1}) (linewidth H_1 = 0.9 mT); g_2 = 1.974; A_2 = 6.0 mT (55.3 10^{-4} cm^{-1}) (linewidth H_2 = 0.8 mT); g_3 = 1.981; A_3 = 5.8 mT (53.6 x 10^{-4} cm^{-1}) (linewidth H_3 = 0.8 mT).

$$g_{iso} = \frac{g_{\parallel} + 2g_{\perp}}{3} \qquad \text{Equation 1}$$

$$A_{iso} = \frac{A_{\parallel} + 2A_{\perp}}{3} \qquad \text{Equation 2}$$

View Article Online
DOI: 10.1039/C9NJ02092F

Finally, the experimental $A_{||}$ value can be compared with that calculated from the additive relationship that links the $A_{||}$ value in V(IV) coordination compounds with the number and type of ligands in the equatorial/basal plane.[25-27] Considering the proposed structure for complex, $A_{||}$ value can be estimated by Equation 3.

$$A_{||_{calculated}} = 2x44.4\cdot10^{-4}(\text{aliphatic imine}) + 2x38.6\cdot10^{-4}(ArO^{-}) = 166\cdot10^{-4}\,cm^{-1} \quad \text{Equation 3}$$

Taking into account the accepted error ca. ± 1.5 x 10^{-4} cm^{-1} per binding group, the calculated value of 166 10^{-4} cm^{-1} shows a good agreement with the experimental one 160.6 x 10^{-4} cm^{-1}.

2.4. Electronic Spectroscopy

Electronic spectra of the complex are recorded in DMSO solution (approximately 10^{-3} M and 10^{-5} M) in the 250-800 nm spectral range and diffuse reflectance spectra of the solid is also measured (see Figure 7).

Spectra of the ligand and the complex in solution do not change during 48 hours, hence denoting their stability in the selected solvent. The absorption bands in solution were assigned with the assistance of theoretical calculations. Calculated electronic transitions are selected according to their oscillator strengths. Experimental and calculated spectra for the complex show a good accordance, as can be seen in Figure 7.

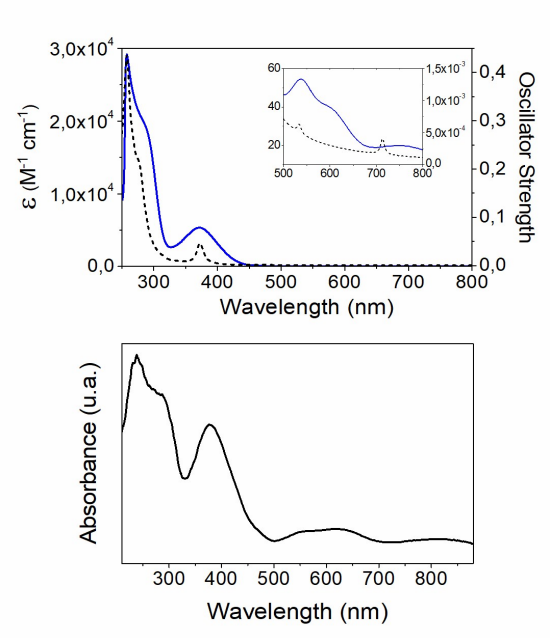

Figure 7: Top: Experimental (solid) and calculated (dashed) electronic spectra of the complex registered for 5x10^{-5} M DMSO solutions. Higher concentration (5x10^{-3} M) was employed to register *d-d* transitions Bottom: Diffuse reflectance spectra of solid sample.

View Article Online
DOI: 10.1039/C9NJ02092F

Table 3 lists experimental bands and calculated electronic transitions for the complex, along with their assignment. As can be seen from the assignment proposed, some experimental bands are described by more than one single electronic calculated transition. Present calculations show that many-body effects are far from negligible as most of calculated transitions are described by several one-electron excitations, thus involving several MO's. To simplify the description of transitions and the corresponding assignment of experimental bands, an arbitrary threshold to the one-electron excitation coefficients obtained from the TD-DFT is imposed. This way, the number of one-electron excitations selected to describe the experimental bands is considerably reduced. Graphical representations of the OM's involved in the electronic transitions of complex are available as ESI (Figure S3). It can be observed in Figure S3 that the $HOMO_{\alpha}$ – 1 in the complex is localized in the two oVA rings and the four O atoms, whereas the $HOMO_{\alpha}$ – 2 is located at the V ion with contributions from the O atoms of the coordination sphere. The $HOMO_{\alpha}$ – 3 is located in the thiophene ring of one ligand only and the $HOMO_{\alpha}$ – 6 is strongly delocalized in the two oVA fragments, the two N atoms, one thiophene moiety and the metal ion. Interestingly, $LUMO_{\alpha}$, $LUMO_{\alpha}$ + 2, $LUMO_{\alpha}$ + 4 and $LUMO_{\alpha}$ + 6 are mainly located on the VO group with minor contributions from the C=N bond, the o-VA rings, the N atoms and the thiophene rings. It is also interesting to note that both $HOMO_{\beta}$ – 3 and $HOMO_{\beta}$ – 6 are localized in the thiophene rings. Finally, the $LUMO_{\beta}$ + 1 is located at the two o-VA rings, the O atoms of the coordination sphere, the C=N atoms and the metal ion.

The characteristic three d-d-bands expected for the V(IV) d^1 ion with a square pyramid coordination sphere are observed for complex in solution.[28-30] In the solid state, however, the bands are less defined, although one absorption at approximately 778 nm and a very broad band with two maxima at 626 nm and 553 nm can be identified.

The differences in intensity and the shifts in the band positions between the diffuse reflectance and UV-Vis spectra are a consequence of the different physical basis of both measurement method, the way in that data is analyzed and the expected solvent effect.[31] The results indicate that there are no significant changes in the metal environment when compared solid samples with solutions. Transitions at higher energy are predicted by calculations but they are expected at a lower wavelength than the solvent cut-off.

View Article Online
DOI: 10.1039/C9NJ02092F

Table 3. Experimental and calculated electronic spectra of the complexes in DMSO solution. Band maxima (calculated from deconvolution) and transition energies are given in nm. Molar absorptivity, in $M^{-1}.cm^{-1}$, and calculated oscillator strength, in atomic units, in parentheses. The proposed assignment is also given. H and L are used as short notation for HOMO and LUMO, respectively, whereas α and β refer to the electronic spin channels, when needed.

Experimental	Calculated	Transition	Assignment
753 (11.4)	713.4 (0.0002)	$H_\alpha - 2 \rightarrow L_\alpha$ $H_\alpha - 2 \rightarrow L_\alpha + 2$	d → d
595 (31.2)	534.0 (0.0001)	$H_\alpha - 2 \rightarrow L_\alpha + 4$	d → d
528 (37.2)	477.6 (0.0008)	$H_\alpha - 2 \rightarrow L_\alpha + 6$	d → d
372 (5.3x10^3)	372.4 (0.0398)	$H_\alpha - 1 \rightarrow L_\alpha$	Ligand-to-metal charge transfer
	281.0 (0.0258)	$H_\beta - 3 \rightarrow L_\beta + 1$	Intra- and interligand
285 (sh)	280.1 (0.0261)	$H_\alpha - 6 \rightarrow L_\alpha$	Ligand-to-metal charge transfer
	275.7 (0.0497)	$H_\beta - 6 \rightarrow L_\beta + 1$	Intra- and interligand
258 *	258.6 (0.0891)	$H_\alpha - 3 \rightarrow L_\alpha + 2$	Ligand-to-metal charge transfer

(*) Poorly-defined maximum due to the solvent cut-off.

2.5. Thermal analysis

The thermal behavior of the complex was studied analyzing the TG and DT data obtained through the incineration of solid in oxygen and nitrogen flux, in order to avoid V(IV) oxidation in the latter case. Thermograms are depicted in Figure S5 (ESI).

The TG and DT curves of the ligand, previously described [21], show the melting point at 70.5°C. Decomposition involving several exothermic processes starts at 165°C with a mass loss of 59% in a first step, assignable to the removal of the substituted benzene ring. In a second step, the loss of the remaining ligand´s fragments lead to a total weight loss of 97%.

For the complex, the TG and DT curves obtained under O_2 flow show two decomposition steps. The first one begins at 211°C (before reaching the melting point), and involves two exothermic processes, with a weight loss of 17.6%. The second step occurs at 370°C with a weight loss of 66.2%. In this case it is observed that the residue corresponds to V_2O_5, as it is confirmed by FTIR. When run under N_2, the thermograms show an endothermic peak corresponding to the melting point of the compound (229°C), followed by an incomplete exothermic decomposition with a weight loss of 78.6% at 800°C.

Results indicate that, even in presence of oxygen, the complex has a good thermal stability.

The melting point value of the complex measured in a Bockmonoscop “M” instrument has some difference with that determined by TG due to the thermal inertia during the heating process in this experiment.

View Article Online
DOI: 10.1039/C9NJ02092F

2.6. Cytotoxicity Assays.

Cytotoxicity studies, determined by the MTT assay, were carried out for $[VO(oVATPNH2)_2]$, free ligand (oVATPNH2) and VO^{2+} ion with three tumor cell lines: MG-63 (human osteosarcoma), MCF7 (breast adenocarcinoma) and MDA-MB-231 (triple negative breast adenocarcinoma) and one normal cell line L929 (mouse derived fibroblast).

Table 4 shows the IC_{50} values and the selectivity index (SI) of $[VO(oVATPNH2)_2]$. As it can be seen, the complex impaired cell viability on MCF7 and MG-63 cells in the range of concentration (25-75 μM) and in the range of 10-45 μM for MDA-MB-231 cells. Besides, $[VO(oVATPNH2)_2]$, displayed an acceptable value of SI (2.45) on triple negative breast adenocarcinoma cell line (MDA-MB-231) since the IC_{50} on tumor cells decreases by 2 times compared to non-tumoral cells.

On the other hand, the IC_{50} values of the free ligand and free metal cations are greater than 100 μM for the three cell lines tested, hence revealing the important role of complexation to modulate the antitumor properties of this kind of compounds.

Table 4. IC_{50} values and SI of complex $[VO(oVATPNH2)_2]$. on MG-63, MCF7, MDA-MB-231 and L929 cell lines after 48 h of incubation.

Cell lines	IC_{50}	SI
MG-63	50.4 ± 8.7	1.41
MCF7	42.3 ± 4.7	1.68
MDA-MB-231	29.0 ± 1.7	2.45
L929	71.0 ± 3.5	

As a whole, our results exhibit the beneficial influence of metal complexation on the anticancer activity as compared with the free ligand and the free metal ion independently. This enhancement has been described for other metal-based compounds.[32-34]

Moreover, these results indicate that the complex displayed a selective action on breast cancer cells mainly on triple negative breast adenocarcinoma cell line. Moreover, the IC_{50} values observed in Table 4 show a good correlation with the anticancer activity compared to other vanadium compounds reported in the literature. In this sense, different oxidovanadium(IV) complexes of salicylaldimines and aromatic heterocycles showed IC_{50} in the range from 53 to 90 μM on MCF-7 cells.[35] Besides, the vanadium(IV) complex with morin exert anticancer activity showing IC_{50} values in the range of 55-65 μM for several breast cell lines.[36]

Nevertheless, some vanadium compounds exhibit lower IC_{50} than $[VO(oVATPNH2)_2]$, as in the case of oxidovanadium(IV) complexes with Knoevenagel condensate Schiff base ligands that have IC_{50} around 20 μM on MCF-7 cells.[37] Besides, different oxidovanadium(IV) compounds

View Article Online
DOI: 10.1039/C9NJ02092F

with imine ligands show very low IC_{50} on MCF-7 cells in the range of 3 to 15 μM but no information ~~available~~ about the cytotoxic effects of these kind of compounds on non-tumoral cells is available.[38] However, some dioxidovanadium(V) complexes with thiosemicarbazones shows variable IC_{50} (range 15-90 μM) on MCF7 cells.[39]

Compared with complexes of the same ligand and other metals, tested in our laboratory , $[VO(oVATPNH2)_2]$, showed higher anticancer activity than $[Zn(oVATPNH2)_2]$, ($IC_{50\ MDA\text{-}MB.231}$ =42 ± 3, $IC_{50\ MCF7=}$ 44 ± 0.2) but lower antitumor actions than $[Cu(oVATPNH2)_2]$, ($IC_{50\ MDA\text{-}MB.231=}$ 23 ± 2, $IC_{50\ MCF7=}$ 14 ± 3).[21]

2.7. Cell migration

Migration is an important property of live cells and critical for normal development, immune response and disease processes such as cancer metastasis and inflammation.[40] The study of cell migration in cancer investigation is of interest as the main cause of death in cancer patients is related to metastatic progression. Therefore, we evaluated the inhibition effect of $[VO(oVATPNH2)_2]$ on cell migration (wound healing assay) on MDA-MB-231 breast cancer cells. Our previous results shows that MDA-MB-231 is the most drug sensitive cell line, therefore we choose it to perform cell migration assay.

Figure 8 shows the wound healing results. As it can be seen, the compound inhibited MDA-MB-231 cell migration in a 60% (10 μM) and 40% (25 μM) compared to the untreated cells. These results are in agreement with our previous findings in which we demonstrated that vanadium-chrysin and vanadium-clioquinol complexes inhibit the cell migration in human cancer cells by inactivation of Focal Adhesion Kinase (FAK).[41,42]

View Article Online
DOI: 10.1039/C9NJ02092F

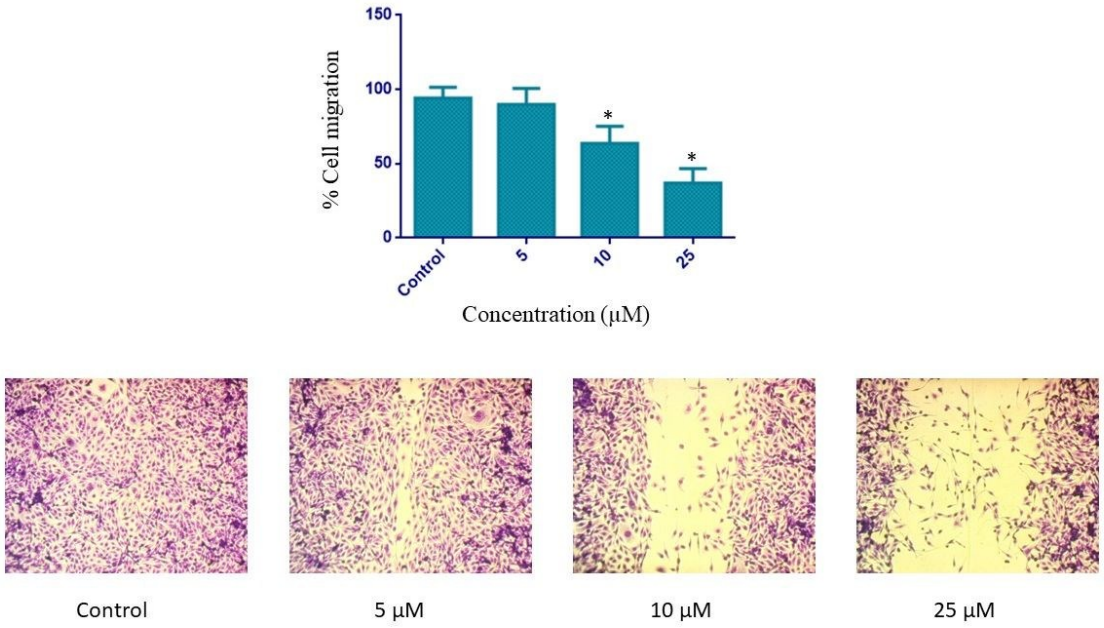

Figure 8. Cell migration study (Wound healing assay) on MDA-MB-231 cells. * p<0.01 differences between control and treatment with compounds.

Mechanism of action

The putative cell death mechanisms triggered by [VO(oVATPNH2)$_2$] on the most drug sensitive cell line (MDA-MB-231) were investigated through the determination of the oxidative stress and an exhaustive study of apoptosis.

2.8. ROS production

Oxidative stress has been reported as one of the most important factors that intervenes in the antitumor activity of vanadium compounds.[19] For a better understanding of the possible mechanism involved in the cytotoxicity of [VO(oVATPNH2)$_2$] in MDA-MB-231 cells, we evaluated the effect of this complex on oxidative stress through the oxidation of the probe DHR-123, a mitochondria-associated probe that selectively reacts with hydrogen peroxide.[43]

Incubation of MDA-MB-231 cells with the complex produced an increment in the ROS production from 10 to 50 μM (p<0.01). Figure 9 shows that after incubation with 10 μM, the complex induced the ROS production (% 150 over basal) whilst at 50 μM this value it increases until 270% (p< 0.01). There results show that the ROS production is, at least partially, one of main mechanisms of action involved in the anticancer activity of [VO(oVATPNH2)$_2$]. Different scientific reports showed similar values of ROS production for other vanadium compounds.[44,45]

View Article Online
DOI: 10.1039/C9NJ02092F

In this way, it can be assumed that the free radicals decrease the concentration of important cellular compounds and impair the antioxidant system, making cells more vulnerable to oxidative damage.

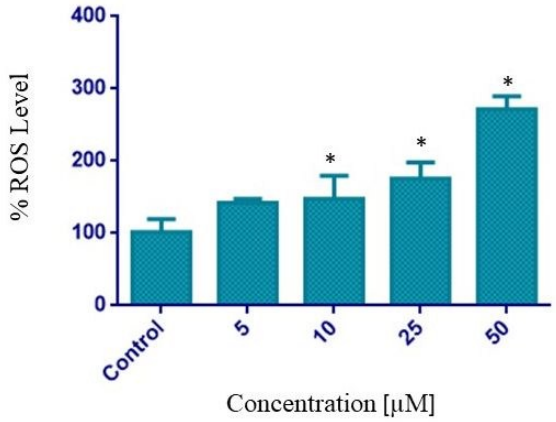

Figure 9. Induction of ROS by [VO(oVATPNH2)$_2$]. in the MDA-MB-231 cell line. The results represent the mean ± SEM (n = 12). Asterisk significant difference versus the control (*p <0.01)

2.9. Apoptosis study

Many scientific articles have shown the important relationship between high levels of ROS and apoptosis induction.[46,47] Regulated cell death requires severe oxidative stress and cytosolic Ca^{2+} overload.[48] Apoptosis is a physiological process of cell death enhanced in the presence of injurious agents. It is characterized by some morphological changes in the nucleus and the cytoplasm. One of the first alterations that can be defined is the externalization of phosphatidylserine at the outer plasma membrane leaflet. Annexin V–FITC is a fluorescent probe with high affinity for phosphatidylserine.

To elucidate the mechanism of cell death induced by the vanadium complex we performed flow cytometry assays using Annexin V–FITC and propidium iodide (PI) staining.

Figure S6 (ESI) depicts the flow cytometry results of the apoptotic process in the presence of [VO(oVATPNH2)$_2$] (2.5, 5, 10 and 25 μM).

In Table 5, it can be seen that the control cultures showed that 9 % of early apoptotic cells were annexin V positive and 2 % of late apoptotic cells were annexin V positive/PI positive. These results denoted an increase in the early and late apoptotic cellular fractions in a concentration dependent manner. At 5 μM, [VO(oVATPNH2)$_2$] resulted in approximately 23 % of early apoptotic cells and 16 % of late apoptotic cells, whereas at 10 μM, the compound produced a striking increase in the fraction of early (34%) and late (28%) apoptotic cells. Besides, at 25 μM, the compound increased the early apoptotic cell fractions up to 43%.

View Article Online
DOI: 10.1039/C9NJ02092F

As can be seen, the percentages of apoptotic cells increased with the concentration of vanadium complex. These results are in accordance with the viability assays, confirming that the deleterious action of $[VO(oVATPNH2)_2]$ is dependent on its concentration in the breast cancer cell line.

Table 5. Percentage of apoptotic cells treated with $[VO(oVATPNH2)_2]$. * significant difference versus the control ($p < 0.01$)

	ANNEXIN V+/PI-	ANNEXIN V+/PI+	ANNEXIN V-/PI+
0 μM	8.4 ± 1.3	2.1 ± 0.6	1.0 ± 0.2
2.5 μM	12.8 ± 0.4	4.4 ± 0.8	1.7 ± 0.2
5 μM	*23.5 ± 5.1	*16.4± 3.1	5.8 ± 1.3
10 μM	*33.9 ± 4.4	*28.2± 4.7	5.2 ± 1.4
25 μM	*42.9± 3.0	*23.6 ± 10.1	3.2 ± 1.7

3. Conclusions

The ligand oVATPNH2 (HL), obtained from the condensation reaction of o-vanillin and 2-thiophenemethylamine is a good chelating agent for vanadyl(IV) ion, leading to the formation of the stable complex $[VO(oVATPNH2)_2]$. HL acts as the monoanion L^- after deprotonation of the OH moiety and coordinates to the metal trough the the phenoxo oxygen and the imine nitrogen atoms, in *trans* position.

Based on spectroscopic analysis and theoretical calculations, a distorted square base pyramidal environment is stablished for the V(IV) ion, with the ligands in the equatorial plane and the oxo group in the apical position.

The relative orientation of thiophene rings prevents the participation of the S atom in the coordination sphere. A *trans* conformation with respect to the pyramid base was proposed as the more stable geometry.

The vibrational (FTIR and Raman) modes of the free ligand are consequently changed upon coordination to the metal and new bands appear as a consequence of metal binding to the donor atoms. EPR spectroscopy results describe the square pyramidal environment for the geometry for the oxidovanadium(IV) monomeric paramagnetic centre. In the electronic spectra the expected *d-d* transitions of complex were identified. Charge transfer and intra- and/or inter-ligand transitions could be assigned in the spectra of the complex. Electronic and EPR results indicate that the coordination environment in the solid is retained in solution.

Cytotoxicity studies on bone (MG-63) and breast cancer cell lines (MCF7 and MDA-MB-231) show that the complex has the strongest anticancer activity on triple negative breast

View Article Online
DOI: 10.1039/C9NJ02092F

adenocarcinoma cell line (MDA-MB-231 cells). Furthermore, the compound inhibits breast cancer cell migration, increases ROS level and induced the activation of programed cell death. Considering the low toxicity of [VO(oVATPNH2)$_2$] and the limitations in the treatment of triple negative breast adenocarcinoma, our results indicate that this complex is an interesting candidate for potential anticancer applications and it would be attractive to test this complex in further in vivo studies for cancer treatments.

4. Experimental

4.1. Synthesis

The solvents and reactants, methanol and acetonitrile (Carlo Erba) and oxovanadium(IV) acethylacetonate (Fluka), were used as provided with no further purification The ligand oVATPNH2 was prepared according with previously reported data.[13]

Elemental analyses were performed in an Exeter CE 440 analyser and melting points were determined in a Bock monoscop “M” instrument.

The complex [VO(oVATPNH$_2$)$_2$] was prepared according the following procedure: 0.50 mmol (0.1236g) of ligand (HL) were dissolved in 10 mL of methanol under stirring and heating. The solution was transferred to a round bottom flask in a reflux set up. Once achieved the reflux temperature, a methanolic solution (5 mL) of VO(acac)$_2$ (0.0658 g, 0.25 mmol) was dropwise added. The system was kept under reflux for one hour and then let to cool gradually until room temperature. A microcrystalline green solid was formed, isolated by filtration and dried in dissector. (Yield: 56%, 0.0779 g, m.p: 236-237°C). Anal. Found: C, 55.72; H, 4.41 N, 4.92; S, 11.38 % Calc. for $C_{26}H_{24}N_2O_5S_2V$: C, 55.81; H, 4.32; N, 5.01; S, 11.46 %.

4.2. Spectroscopy

Infrared spectra of solid samples (KBr pellets) were recorded with a Bruker Equinox 55 instrument in the 4000-400 cm^{-1} region. Raman spectra were measured with a WITEC alpha 300 RA spectrophotometer, using laser excitation wavelength of 532 nm and a 20x objective lens.

Electronic spectra of the ligand and the complex were recorded in solution of dimethyl sulfoxide (DMSO), using 10 mm quartz cells in the spectral range from 190 to 800 nm. Diffuse reflectance spectra (convert in absorbance from Kubelka-Munk function) in the 250 - 800 nm range were recorded using $BaSO_4$ pellet as a reference with an integrating sphere attachment. Both spectra were registered in a Shimadzu UV-2006 spectrophotometer.

X-band EPR spectra were acquired on a polycrystalline samples and frozen glassy solutions by using a Bruker EMX spectrometer, equipped with a Bruker ER 036TM NMR-teslameter and an

View Article Online
DOI: 10.1039/C9NJ02092F

Agilent 53150A microwave frequency counter. Variable temperature experiments were precisely controlled by a Bruker ER 4131VT accessory by using the combined action of a liquid nitrogen evaporator, a heater and the BVT3000 temperature controller. A flat quartz cell was used for room-temperature studies in solution, whereas the solvents mixture was quickly frozen inside the standard quartz tube in the experiments at 120 K. SimFonia program [49] was used to perform the simulated spectra and graphics were carried out with Kaleidagraph v4.1.[50] Experimental details are given in figure captions.

4.3. Computational methods.

The structures of the complex was optimized using the Becke's three parameters hybrid density functional [51] with the gradient-corrected correlation functional due to Lee, Yang, and Parr [52] as implemented in of the ORCA program.[53] The Def2-TZVP basis set of triple-zeta quality was used for all the atoms.[54] Based on spectroscopic results, a square pyramidal geometry were taken as starting geometry. Optimizations were conducted in the gas phase.

To verify whether the optimized geometries are local minima or saddle points on the potential energy surface of the molecules the eigenvalues of the Hessian matrix of the total energy with respect to the nuclear coordinates were calculated. Those eigenvalues were then transformed to harmonic vibrational frequencies, which were further used to aid in the assignment of the experimental vibrational frequencies. No factors were used to scale calculated frequencies.

The electronic spectrum of the complex was calculated using the hybrid PBE0 functional [55] as implemented in the ORCA program. The Def2-TZVP basis sets were used for the calculation, too. Solvent effects were included implicitly through the Conductor-like Screening Model (COSMO)[56] as implemented in the ORCA program.

4.4. Thermal analysis.

The thermal analysis (TG and DT) has been performed using Shimadzu TG-50 and DT-50 units, in a 25° to 800 ºC temperature range at a heating rate of 5 ºC min^{-1}. Oxygen flow of 80 mL min^{-1} was employed in every measurement and nitrogen flow was also used for the complex sample.

4.5 Biological assays.

4.6.1. Cell line and growth conditions

MCF-7 (breast) cancer cells were grown in DMEM (Gibco, Gaithersburg, MD, USA) containing 10 % FBS (Internegocios), 100 U/mL penicillin, and 100 µg/mL streptomycin at 37° C in a 5 % CO_2 atmosphere whilst MDA-MB-231 (triple negative breast) were grown in F12-DMEM (Gibco,

View Article Online
DOI: 10.1039/C9NJ02092F

Gaithersburg, MD, USA). Cells were seeded in a 75-cm^2 flask, and when 70–80 % of confluence was reached, cells were subcultured using 1 mL of TrypLE ™ per 25-cm^2 flask. For experiments, cells were grown in multiwell plates. When cells reached the desired confluence, the monolayers were washed with PBS and were incubated under different conditions according to the experiments. All the cell lines were purchased from ATCC (American Type Culture Collection).

4.6.2. Cell viability study: 3-(4,5-Dimethylthiazol-2-yl)-2,5-diphenyltetrazolium bromide (MTT) assay

The MTT assay was performed according to Mosmann.[57] Briefly, cells were seeded in a 96-well dish for 24 h, and treated with different concentrations of the tested compound (1-50 μM) at 37° C for 48 h. Afterward, the medium was changed and the cells were incubated with 0.5 mg/mL MTT under normal culture conditions for 3 h. Cell viability was marked by the conversion of the tetrazolium salt MTT to a colored formazan by mitochondrial dehydrogenases. Color development was measured spectrophotometrically with a microplate reader (model 7530, Cambridge Technology, USA) at 570 nm after cell lysis in DMSO (100 μL per well). Cell viability was plotted as the percentage of the control value.

4.6.3 Wound healing assay

Cells were grown in a 12 well cell culture plates with complete DMEM including 10% FBS, until 100% of confluence. The monolayer was scratched and washed with PBS to remove non-adherent cells. Then, the cells were treated with the complex for 48 hours. After this time, the monolayer was washed with PBS and stained with Giemsa. Digital images were taken using an Olympus BX51 inverted microscope with a digital camera. The inhibition of cell migration was analyzed with ImageJ software. The percentage (%) of migration was calculated using the following formula: 100-(final area/initial area × 100%).

4.6.4 Determination of ROS production

Oxidative stress in MDA-MB-231 cells was evaluated by measurement of intracellular production of ROS after incubation of the cell monolayers with different concentrations of [VO(oVATPNH2)$_2$] for 24 h at 37 °C. ROS generation was determined by oxidation of DHR-123 (Sigma-Aldrich, San Luis, USA) to rhodamine by spectrofluorimetry, as we have previously described. [58]

View Article Online
DOI: 10.1039/C9NJ02092F

4.6.5 Apoptosis study

Cells in early and late stages of apoptosis were detected with annexin V–FITC and PI staining. Cells were treated with 0, 2.5, 5, 10 and 25 μM of [$VO(oVATPNH2)_2$] and were incubated for 48 h prior to analysis. For the staining, cells were washed with PBS and adjusted to a concentration of 1 x 10^6 cells per milliliter in binding buffer.

Cells were analyzed using a BD Accuri C6 Plus ™ flow cytometer (BD Biosciences, USA) and BD Accuri C6 Plus Software. For each analysis, 10,000 counts, gated on a forward scatter versus side scatter dot plot, were recorded. Four subpopulations were defined in the dot plot: the undamaged vital (annexin V negative/PI negative), the vital mechanically damaged (annexin V negative/PI positive), the apoptotic (annexin V positive/PI negative) and the secondary necrotic (annexin V positive/PI positive).

Electronic Supplementary Information

Relevant geometrical parameters for the complex (Tables S1), Vibrational (FTIR, Raman) spectroscopic data (Table S2), EPR spectra (Figures S1 and S2), MOs involved in relevant electronic transitions of the complex (Figure S3), TG/DTA thermograms (Figure S4) and apoptosis plots (Figure S5) are available as ESI.

Conflict of interest

There are no conflicts of interest to declare.

Acknowledgments

This work was supported by CONICET-CCT- La Plata (PIP 0651 and 0034), ANPCyT (PICT 2016-1574) and UNLP (11/ X763) Argentina and also by Consejería de Educación CyL and FFEDER BU076U16, BU022G18 and Ministerio de Economía y Competitividad CTQ2016-75023-C2-1-P and CTQ2015-70371-REDT MetDrugs Network (Spain).

R.P.D, I.E.L, B.S.P.C and A.C.G.B are members of the Researcher Career of CONICET. M.R.R, L.M.B. are Doctoral Fellows and J.D.P. is Post-doctoral Fellow of CONICET. The authors thank Dr. David Ibáñez Martinez (Department of Chemistry, Universidad of Burgos, España) for Raman spectra.

View Article Online
DOI: 10.1039/C9NJ02092F

References

1- J. Costa Pessoa, S. Etcheverry and D. Gambino, *Coord. Chem. Rev.* 2015, **301-302**, 24-48.

2- D. Rehder, *Metallomics*, 2015, **7**, 730-742.

3- C. C. Mc Lauchlan and D. C. Crans, *Dalton Trans.* 2013, **42(33)**, 11744-11748.

4- A. C. González-Baró, V. Ferraresi-Curotto, R. Pis-Diez, B. S. Parajón-Costa, J. A. L. C. Resende, F. C. S. de Paula, E. C. Pereira-Maia and N. A. Rey, *Polyhedron*, 2017,**135**, 303-310.

5- D. C. Crans, J. J. Smee, E. Gaidamauskas and L. Yang *Chem. Rev.* 2004**, 104,** 849-902.

6- M. Khorshidifard, H. A. Rudbari, Z. Kazemi-Delikani, V. Mirkhani and R. Azadbakht, *J. Mol. Struct*. 2015, **1081**, 494–505.

7- E. Kioseoglou, S. Petanidis, C. Gabriel and A. Salifoglou, Coord. Chem. Rev. 2015, **302-302**, 87-105.

8-T. Storr, K. H. Thompson and C. Orvig, *Chem. Soc. Rev*. 2006, **35**, 534–544.

9- M. Sutradhar and A. J. L. Pombeiro, *Coord. Chem. Rev.* 2014, **265** 89–124.

10- S. Kumar, D.N. Dahr, and P.N. Saxena, *J.Ind.Sci.Res.* 2009, **68**, 181-187.

11- W. Al Zoubi, *Int. J. Org. Chem.* 2013, **3**, 73-95.

12- X. Liu , C. Manzur , N. Novoa, S. Celedón, D. Carrillo and J. R. Hamon, *Coord. Chem. Rev.* 2018, **357,** 144-172.

13- M. R. Rodríguez, J. Del Plá, O. E. Piro, G. A. Echeverría, G. Espino, R. Pis-Diez, B. S. Parajón-Costa and A C. González-Baró*, J. Mol. Struct.* 2018, **1165**, 381-390.

14- A. B. Gündüzalp, N. Özbek, N. Karacan, *Med. Chem. Res.* 2012, **21**, 3435-3444.

15- M. A. Malik, O. A. Dar, P. Gull, M.Y. Wani and A. A. Hashmi, *Med. Chem. Comm.* 2018, **9(3**), 409–436.

16- L. N. F. Cardoso, T. C. M. Nogueira, F. A. R. Rodrigues, A. C. Aragão Oliveira, M. C. dos Santos Luciano, C. Pessoa and M. V. N. de Souza, *Med. Chem. Res.* 2017, **26(8)**, 1605–1608.

17- S. Santosh Kumar, K. Priyadarsini and K. B Sainis, *Redox Report* , 2002, **7**, 35-40.

18- A. Hameed, M. al-Rashida, M. Uroos, S. Abid Ali and K. M. Khan, Expert. Opin. Ther. Pat. 2017, 27(1), 63–79.

19- I. E. León, J. F. Cadavid-Vargas, A. L. Di Virgilio and S. B. Etcheverry, *Curr. Med.Chem.* 2017, **24(2)**, 112-148.

20- J. A. de la Mare, L. Contu, M. C. Hunter, B. Moyo, J. N. Sterrenberg, K. C. Dhanani, L. Z. Mutsvunguma and A. L. Edkins. *Recent Pat. Anticancer Drug Discov*. 2014, **9(2)**, 153-175.

21- M. R. Rodríguez, J. Del Plá L. M. Balsa, I. E. León, O. E. Piro, G. A. Echeverría, J. García-Tojal, R. Pis-Diez, B. S. Parajón-Costa and A. C. González-Baro, *New J. Chem.* 2019, **43**, 7120-7129.

View Article Online
DOI: 10.1039/C9NJ02092F

22- D. Lin-Vien, N. B. Colthup, W. G. Fately and J. G. Grasselli in: *Infrared and Raman Characteristic Frequencies of Organic Molecules*, Academic Press, Boston, 1999.

23- K. Nakamoto, in: *Infrared and Raman Spectra of Inorganic and Coordination Compoun*ds, Sixth ed., J. Wiley & Sons, Inc., Hoboken, New Jersey, 2009.

24- A. C. González-Baró, R. Pis-Diez, C. A. Franca, M. H. Torre and B. S. Parajón-Costa, *Polyhedron*, 2010, **29**, 959-968.

25- K. Wuthrich, *Helv. Chim. Acta,* 1965, **48**, 1012-1017,

26- N. D. Chasteen, in *Biological magnetic resonance,* Berliner, L. J.; Reuben, J. (Eds.), Vol. 3; Plenum Press: New York, 1981.

27- T. S. Smith II, R. LoBrutto and V. L. Pecoraro, *Coord. Chem. Rev.* 2002, **228**, 1-18

28- A. B. P. Lever in *Inorganic electronic Spectrocopy*, 2nd Ed. Elsevier, Amsterdam, 1984.

29- J. Ballhausen, H. B. Gray *Inorg. Chem.* 1962, **1(1)**, 111-122.

30- J. Selbin, G. Maus and D. L. Johnson, *J. Inorg. Nucl. Chem* 1967, **29**, 1735-1744.

31- G. Kortüm in *Reflectance Spectroscopy. Principles, Methods, Applications*. Springer-Verlag, New York Inc. 1969.

32- A. Matesanz , E. Jimenez-Faraco, M. C. Ruiz, L. M. Balsa, C. Navarro-Ranninger, I. E. León and A. G. Quiroga, *Inorg. Chem. Front*. 2018, **5**, 73-83.

33- I. E. Leon, J. Cadavid-Vargas, I.Tiscornia, V.Porro, S. Castelli, P. Katkar, A. Desideri, M. Bollati-Fogolin and S. Etcheverry *J. Biol. Inorg. Chem*. 2015, **20(7)**, 1175-1191.

34- J. Grau, C. Renau, A. B. Caballero, A. Caubet, M. Pockaj, J. Lorenzo and P. Gamez, *Dalton Trans.* 2018, **47(14)**, 4902-4908.

35- I. Correia, S. Roy, C. P. Matos, S. Borovic, N. Butenko, I. Cavaco, F. Marques, J. Lorenzo, A. Rodríguez, V. Moreno and J. C: Pessoa *J. Inorg. Biochem.* 2015, **147**, 134-146.

36- 32- L. G. Naso , L. Lezama, T. Rojo, S. B. Etcheverry, M. Valcarcel, M. Roura, C. Salado, E. G. Ferrer, P. A. Williams *Chem Biol Interact.* 2013, **206(2)**, 289-301.

37- R. Paulpandiyan and N. Raman, *Bioorg Chem.* 2017, **73,** 100-108.

38- L. P. Lu, F. Z. Suo, Y. L. Feng, L. L. Song, Y. Li, Y. J. Li and K. T. Wang, *Eur J Med. Chem.* 2019, **7,**176:1-10

39- S. Saswati, P. Adão, S. Majumder, S. P. Dash, S. Roy, M. L. Kuznetsov, J. Costa Pessoa, C. S. B. Gomes, M. R. Hardikar, E. R. T. Tiekink and R. Dinda, *Dalton Trans.* 2018, **47(33)**, 11358-11374

40- C. R. Justus, N. Leffler, M. Ruiz-Echevarria, and L. V. Yang, *J. Vis. Exp.* 2014; **88**, 51046.

41- I. E. León, P. Díez, S. B. Etcheverry and M. Fuentes, *Metallomics*, 2016, **8**, 739-749.

42- I. E. León, P. Díez, E. J. Baran, S. B. Etcheverry and M. Fuentes, *Metallomics*, 2017, **9**, 891–901.

View Article Online
DOI: 10.1039/C9NJ02092F

43- M. A. M. Capella, L. S. Capella, R. C. Valente, M. Gefe and A. G. Lopes, *Cell. Biol. Toxicol.* 2007, **23**, 413–420.

44- J. X. Wu, Y. H. Hong and X. G. Yang, *J. Biol. Inorg. Chem*. 2016, **21(8)**, 919-929.

45- S. Kowalski, S. Hać, D. Wyrzykowski, A. Zauszkiewicz-Pawlak, I. Inkielewicz-Stępniak, *Oncotarget*, 2017, **8(36)**,60324-60341.

46- L. S. Flocke, R. Trondl, M. A. Jakupec and B. K. Keppler, *Invest. New Drugs* 2016, **34**, 261–268.

47- A. Terenzi, C. Pirker, B. K. Keppler and W. Berger, *J. Inorg. Biochem.* 2016, **165**, 71-79.

48- T. Vanden Berghe, A. Linkermann, S. Jouan-Lanhouet, H. Walczak, P. Vandenabeele, *Nat. Rev. Moll. Cell. Biol.* 2014, **15**, 135-147.

49- SimFonia v1.25, Bruker Analytische Messtecnik GmßH, 1996.

50- Kaleidagraph v3.5 Synergy Software, 2000.

51- D. Becke, *J. Chem. Phys.* 1993, **98**, 5648-5652.

52- C. Lee, W. Yang, R. G. Parr, *Phys. Rev*. 1988, **B 37**, 785-789.

53- F. Neese, *Wiley Interdiscip. Rev. Comput. Mol. Sci*. 2012, **2**, 73-78.

54- F. Weigend and R. Ahlrichs, *Phys. Chem. Chem. Phys.* 2005, **7**, 3297-3305.

55- C. Adamo and V. Barone, *J. Chem. Phys.* 1999, **110**, 6158-6170.

56- A. Klamt and G. Schüürmann, *J. Chem. Soc., Perkin Trans.* 1993, **2**, 799-805.

57- T. T. Mosmann, J. Immunol. Methods, 1983, **65**, 55-63.

58- I. E. Leon, A. L. Di Virgilio, V. Porro, C. I. Muglia, L. G. Naso, P. A. M: Williams, M. Bollati-Fogolin and S. B. Etcheverry, *Dalton Trans*. 2013, **42**, 11868-11880.

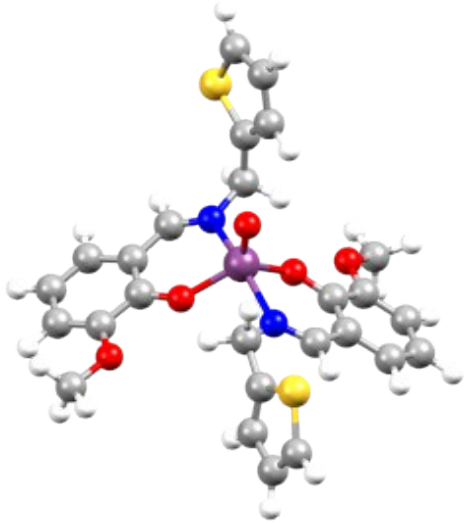

[VO(oVATPNH2)2]

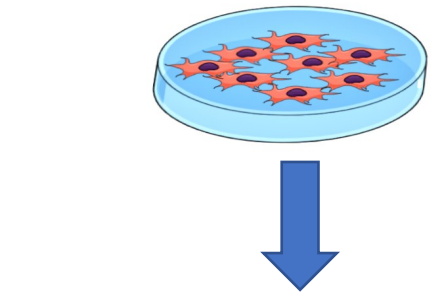

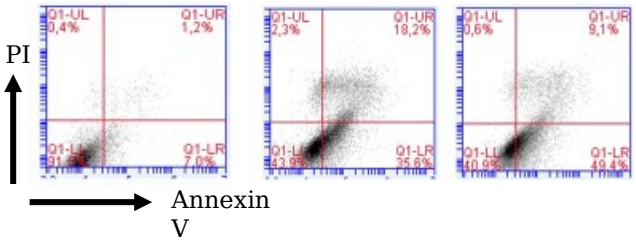

New vanadium complex was synthesized and fully characterized showing promising anticancer activity on triple negative breast cancer cells.